A SANS Study of 3PEG−$LiClO_4$−TiO_2 Nanocomposite Polymer Electrolytes

C. Karlsson,[†] A. S. Best,[‡] J. Swenson,*[,†] J. Kohlbrecher,[§] and L. Börjesson[†]

Department of Applied Physics, Chalmers University of Technology, SE-412 96 Göteborg, Sweden; Delft Institute for Sustainable Energy, Laboratory for Inorganic Chemistry, Delft University of Technology, Julianalaan 136, 2628 BL, Delft, The Netherlands; and Paul Scherrer Institute, CH-5232 Villigen PSI, Switzerland

Received February 28, 2005; Revised Manuscript Received May 19, 2005

ABSTRACT: Nanocomposite polymer electrolytes based on a fully amorphous polymer electrolyte (trihydroxypoly(ethylene oxide-*co*-propylene oxide), known as 3PEG, with $LiClO_4$ salt) were studied by means of small-angle neutron scattering with the aim to clarify how the filler particles (nanosized TiO_2 or Al_2O_3) are distributed in the polymer. The scattering data show that the particles are not well dispersed but aggregate in fractal, polymer-like structures. The structures, with a fractal dimension of ∼2 on length scales from 100 nm up to at least 400 nm, consist of branched chains which are about 1−2 primary particles wide (∼40 nm for TiO_2 and ∼30 nm for Al_2O_3). The obtained results provide structural support for the hypothesis of earlier works that the ionic conductivity increase observed in nanocomposite polymer electrolytes is due to the formation of a percolating layer close to the filler particles with higher conductivity.

1. Introduction

Polymer electrolytes have attracted much research effort during the past decades, mainly due to their potential use in various electrochemical applications, for instance as rechargeable lithium batteries.[1,2] The great challenge is to find materials that combine high ionic conductivity with suitable mechanical and electrochemical properties. To achieve this, the early polymer electrolyte concept based on an alkali metal salt (e.g., $LiClO_4$) dissolved in high molecular weight poly(ethylene oxide) (PEO) has been developed in several directions. Blending inorganic materials into a polymer electrolyte is a method that has been used since the 1980s when micrometer-sized ceramic particles (for instance Al_2O_3) were added to polymer electrolytes in order to improve the mechanical properties.[1,3,4] In some instances also the ionic conductivity increased (see for instance ref 5). Later, nanosized particles were used in PEO-based electrolytes, and room temperature conductivities of the order 10^{-5} S/cm were obtained.[6,7] This value of conductivity is higher than what has been observed in corresponding composites with micrometer-sized fillers.[6] An increase in the transport number of lithium has also been observed in nanocomposites,[7] but a rigorous study is yet to be undertaken, as a function of salt concentration and polymer type. The origin of the conductivity enhancement in micro- and nanocomposite polymer electrolytes is yet to be clarified. Since ionic conduction in polymer electrolytes is believed to take place predominantly in the amorphous phase,[8] the reduction of crystallinity upon the addition of filler can explain some of the conductivity increase in systems based on semicrystalline polymers, such as PEO. However, other mechanisms must be involved since conductivity increases are observed above the melting point of the PEO−salt complex[6,7] and also in composites based on amorphous polymers, at least for certain salt and filler concentrations.[9] Wieczorek et al. showed that effective medium theory (EMT) models, in which dispersed filler particles are assumed to be surrounded by interface regions with an enhanced conductivity over the bulk electrolyte, can be used to describe the conductivity behavior.[10] However, they did not address the question of why the conductivity is different in these interfacial regions. Several authors have later pointed out the importance of Lewis acid−base interactions between filler, salt, and polymer and the local structure that surrounds the filler particles when describing the conductivity increases.[7,11−13] Best et al. showed, by using a simple electrostatic model, that lithium cations experience the same potential at TiO_2 filler surfaces as at the polymer, which means that lithium ions can move between these sites with a lowered activation energy barrier.[14] In a recent paper the same authors propose that the conductivity increase is due to the formation of percolating interface regions which allows the formation of conduction pathways near filler particles.[15] However, no study of the actual particle size and distribution of the filler particles in polymer electrolytes has been performed. The question of whether the particles are dispersed individually or if they form larger aggregates within the polymer electrolytes is yet to be addressed.

Small-angle neutron or X-ray scattering (SANS or SAXS) are suitable techniques for studying the structure of materials on length scales of the order 1−400 nm. The SANS technique is therefore an appropriate methodology for an investigation of the distribution of the filler particles in nanocomposites. SANS experiments measure the coherent macroscopic differential scattering cross section, which for an isotropic two-phase system with identical and spherical symmetric particles dispersed in a matrix is given by[16]

[†] Chalmers University of Technology.
[‡] Delft University of Technology.
[§] Paul Scherrer Institute.
* Corresponding author: e-mail f5xjs@fy.chalmers.se.

10.1021/ma050417v CCC: $30.25
Published on Web 06/23/2005

$$\left[\frac{d\Sigma}{d\Omega}(Q)\right]_{coh} = \frac{1}{V}\left[\frac{d\sigma}{d\Omega}(Q)\right]_{coh} = n_p V_{part}^2 (\Delta\rho)^2 |F(Q)|^2 S(Q) \quad (1)$$

where V is the sample volume, n_p is the number density of particles, V_{part} is the volume of one particle, $\Delta\rho = \rho_{particle} - \rho_{matrix}$ is the contrast, or the difference in scattering length density, between the two phases (the scattering length density is assumed to be homogeneous in each phase), $F(Q)$ is the particle form factor, and $S(Q)$ is the interparticle structure factor, which depends on the distribution of the particles in the matrix (Q is the magnitude of the scattering vector and is given by $Q = |\vec{Q}| = |\vec{k} - \vec{k}'|$, where $\vec{k}$ and $\vec{k}'$ are the wave vectors of incident and scattered neutrons, respectively). The scattering length density is calculated according to[17]

$$\rho = \frac{\delta N_A}{M}\sum_i b_i \quad (2)$$

where δ is the macroscopic density, N_A is the Avogadro constant, M is the molecular weight of a scattering unit, and b_i is the scattering length of the ith atom in the scattering unit.

For fractal structures it has been shown that in the region $Qa \gg 1$, where a is the length scale of the fractal scattering objects, the SANS cross section follows a power law[19,20]

$$\left[\frac{d\Sigma}{d\Omega}(Q)\right]_{coh} \sim Q^{-D} \quad (3)$$

where D is the mass fractal dimension ($1 \le D \le 3$) of the scattering objects. Thus, the slope of the measured intensity vs Q in a log−log plot gives the fractal dimension. For instance, Gaussian polymer chains give a slope of -2 ($D = 2$). More close-packed, treelike structures result in slopes steeper than -2 ($D > 2$), while more stretched, chainlike structures result in slopes less steep than -2 ($D < 2$).[19] Structures consisting of uniformly dense objects (that is $D = 3$) may have fractal surfaces characterized by the surface fractal dimension D_S ($2 \le D_S \le 3$). For such objects the power law given in eq 3 is normally rewritten as $[d\Sigma/d\Omega]_{coh} \sim Q^{D_S-6}$ in order to relate the exponent to the fractal dimension of the surface. In the case of dense objects with smooth surfaces and sharp boundaries (that is $D_S = 2$), a slope of -4 ($D = 4$) is obtained.

No SANS or SAXS studies with focus on polymer nanocomposites have, to our knowledge, previously been performed. However, there have been a number of SANS and SAXS studies[18−21] in the field of filled polymers,[22] where the purpose of the filler (not necessarily nanosized) primarily is to enhance the mechanical properties. In these applications silica, either mixed in or precipitated in situ, and carbon black are the most common filler materials. It has been shown that the morphology of carbon black filled samples is rather complex with structures on several length scales.[19,23] The morphology of composites containing silica depends on the preparation conditions.[21,24−26] For instance, when 10 nm silica particles coated with MPTS (methacryloxypropyltrimethoxysilane) are used, the particles are well dispersed in the polymer matrix, while uncoated particles form larger aggregates.[25] When the silica is formed in situ, the preparation conditions are perhaps even more important for the resulting morphology (see for instance ref 27, in which silica is formed by precipitation from tetraethoxysilane).

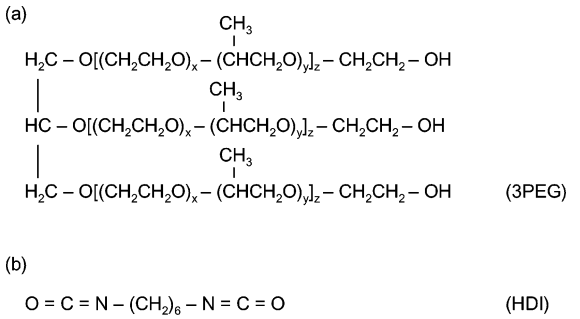

Figure 1. Chemical structure of (a) 3PEG and (b) hexamethylene diisocyanate (HDI).

In this work, we have investigated 3PEG (trihydroxypoly(ethylene oxide-*co*-propylene oxide))-based polymer electrolytes composited with nanostructured Al_2O_3 and TiO_2 by means of SANS in order to elucidate how the filler particles are dispersed into the polymer matrix. We show that the particles are not well dispersed, but instead aggregate in fractal, polymer-like structures.

2. Experimental Section

Nanocomposite polymer electrolytes based on fully amorphous 3PEG, with an ethylene/propylene group ratio of 3:1, were prepared by dissolving dried lithium perchlorate ($LiClO_4$, Fluka, 99% purity) at a salt concentration of 1.5 mol/kg in the carefully washed and dried 3PEG polymer (average molecular weight 7000 g/mol) at an elevated temperature. The polymer−salt complex was then dried for a week at 60 °C prior compositing with nanofillers. Figure 1a shows the chemical structure of 3PEG. Nanosized TiO_2 (Degussa P25, nominal particle diameter 21 nm)[28] or Al_2O_3 (Degussa Aluminoxid C, nominal particle diameter 13 nm) was dried overnight at 250 °C in an oxidizing atmosphere and added to the polymer or polymer−salt complexes. All samples were cured using hexamethylene diisocyanate (HDI, Aldrich, used as received) with Thorcat535 catalyst (Thor Chemical Co., used as received). The chemical structure of HDI is shown in Figure 1b. After curing, cross-links between the end groups of 3PEG are formed. Samples were prepared with 10 and 20 wt % filler, which correspond to about 3 and 6 vol % (TiO_2) or 3 and 7 vol % (Al_2O_3), respectively. The preparation procedure is described in further detail in refs 9 and 14.

Small-angle neutron diffraction experiments were performed using the SANS instrument at the Swiss Spallation Neutron Source, Paul Scherrer Institute, Villigen, Switzerland. The SANS instrument is described in detail in ref 29. The rubberlike 3PEG samples (thickness 2 mm) were placed in open air directly in the beam. Three different wavelength (λ), collimation tube length (L_C), and sample-to-detector distance (L_{SD}) settings were used in order to cover the required scattering vector range ($0.0015\ Å^{-1} < Q < 0.20\ Å^{-1}$). The different settings and corresponding Q ranges as well as scattering curves from two of the samples are shown in Figure 2a.

The measured intensity was corrected for background and detector dead-time and efficiency and then isotropically averaged using routines in the BerSANS package.[30] The corrected intensity in the detector pixel ij, corresponding to scattering vector $\vec{Q}_{ij}$, was calculated according to[30,31]

$$I_{corr}(\vec{Q}_{ij}) = \frac{\dfrac{I_S - I_{Cd}}{T_S} - \dfrac{I_{SB} - I_{Cd}}{T_{SB}}}{\dfrac{I_W - I_{Cd}}{T_W} - \dfrac{I_{WB} - I_{Cd}}{T_{WB}}} \quad (4)$$

where I_S, I_{SB}, I_W, and I_{WB} are the measured intensities from the sample, sample background, water, and water background,

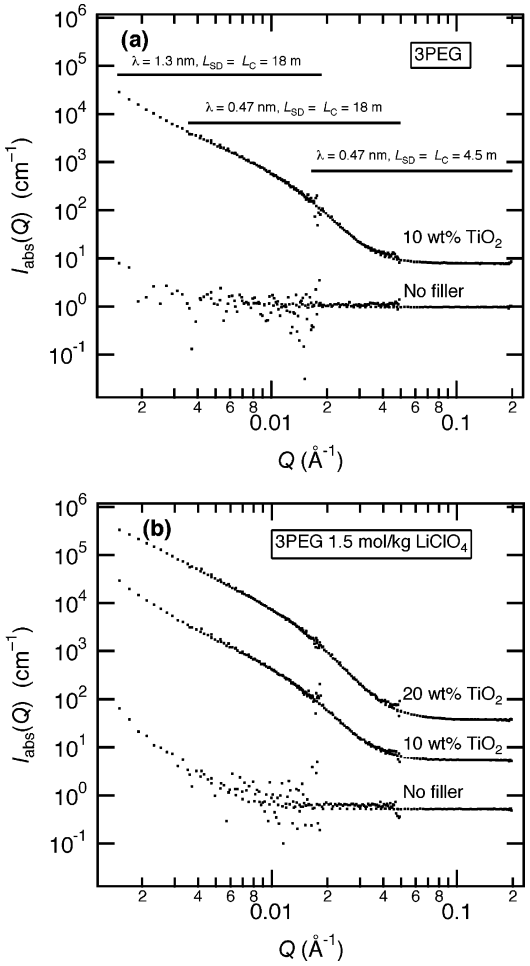

Figure 2. Absolute SANS intensity for 3PEG samples filled with TiO_2. Salt-free compositions are shown in (a), while (b) shows the compositions containing salt. The 10% and 20% filler scattering curves are, for clarity, shifted vertically by multiplication by 10 and 100, respectively. The Q ranges covered by different instrument settings are indicated in (a).

respectively (all normalized to beam monitor counts and corrected for detector dead time) and T_S, T_{SB}, T_W, and T_{WB} are the corresponding transmissions. By radial averaging of $I_{corr}(\bar{Q}_{ij})$ the corrected, radially averaged intensity $I_{corr}(Q)$ was obtained, from which the intensity in absolute units (cm^{-1}) was calculated according to[30,32]

$$I_{abs}(Q) = \frac{d\Sigma}{d\Omega}(Q) = I_{corr}(Q)\frac{V_W}{V_S}g(\lambda)\frac{1-T}{4\pi d_W T} \quad (5)$$

where V_W is the water volume, V_S the sample volume, $g(\lambda)$ a factor that corrects for inelasticity effects ($g = 1.338$ at $\lambda = 0.47$ nm), T the water transmission, and d_W is the thickness of the water standard sample.

3. Results

Figure 2a shows the SANS intensity from pure 3PEG and 10 wt % TiO_2 filled 3PEG. From the pure 3PEG sample there is hardly any scattering apart from the incoherent background, indicating that the sample is homogeneous on the probed length scales (3−400 nm). The filled sample, on the other hand, shows significant small-angle scattering below $Q = 0.05$ Å^{-1}. At around $Q = Q^*$ the slope of the intensity curve changes. No low-Q plateau can be observed within the Q range of the experiment.

Figure 2b shows the SANS intensity from samples with salt added (1.5 mol/kg $LiClO_4$). For the unfilled sample there is some scattering in the low-Q region which is not present in the salt-free 3PEG. This indicates the presence of inhomogeneities due to the salt on length scales of the order of at least $2\pi/0.002$ Å = 300 nm. Previous studies of polymer electrolytes of relatively low salt concentrations have indicated that the salt ions may be inhomogeneously distributed into salt-rich and salt-poor regions.[33−36] The observed small-angle scattering may then reflect lower limits of a typical size of these regions or a typical distance between these regions.

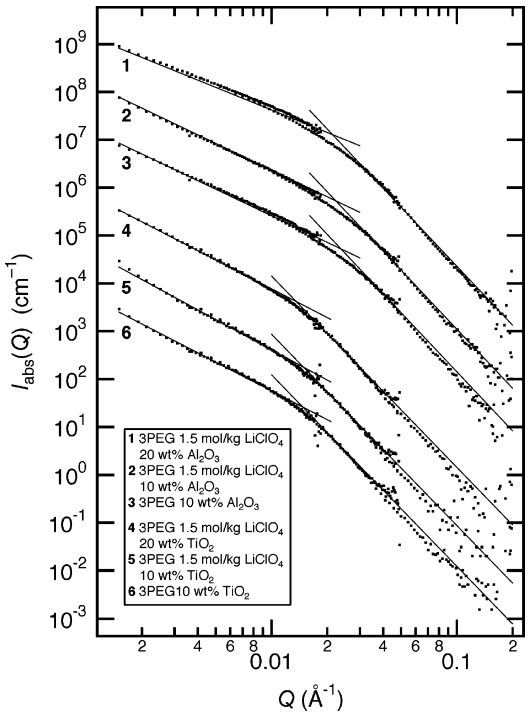

Figure 3. Same data as in Figure 2 but with the background subtracted. Also shown are data from samples containing Al_2O_3 filler. The scattering curves are displaced vertically by factors of 10 for clarity. The slopes of the lines are given in Table 1.

In Figure 3 the data from Figure 2 are plotted with a high-Q background subtracted, corresponding to the level at high Q that should mainly be due to incoherent scattering. Also included are data from samples with Al_2O_3 as filler material instead of TiO_2. For the samples containing Al_2O_3 the scattering extends to somewhat higher Q values, indicating that the Al_2O_3 particles are smaller than the TiO_2 particles. The solid lines of Figure 3 are fitted curves of the power-law form

$$I_{abs}(Q) = CQ^p \quad (6)$$

which were used to determine the slope p of the intensity curve above and below the crossover Q^* for each composition. Numerical values of the slopes and crossover scattering vectors are shown in Table 1.

The fact that no low-Q plateau can be seen in the scattering from any filled sample, with or without salt, shows that the filler particles aggregate and thus impossibly can be well dispersed 21 nm spheres in the TiO_2-filled composites. The same applies for the Al_2O_3-filled composites. Attempts were made to fit the data to calculated form factors for spherical or elliptical particles but failed.

Thus, it is likely that the particles form aggregates. The behavior observed here has earlier been found in

Table 1. Slopes *p* of the Power Laws (Solid Lines) in Figure 3[a]

	low-Q slope	high-Q slope	Q^* (Å^{-1})
3PEG 10 wt % TiO_2 (6)	-2.0 ± 0.1	-4.0 ± 0.1	0.015 ± 0.002
3PEG 1.5 mol/kg $LiClO_4$ 10 wt % TiO_2 (5)	-2.1 ± 0.1	-4.0 ± 0.1	0.015 ± 0.002
3PEG 1.5 mol/kg $LiClO_4$ 20 wt % TiO_2 (4)	-2.0 ± 0.1	-4.0 ± 0.1	0.014 ± 0.002
3PEG 10 wt % Al_2O_3 (3)	-1.85 ± 0.10	-4.1 ± 0.1	0.024 ± 0.003
3PEG 1.5 mol/kg $LiClO_4$ 10 wt % Al_2O_3 (2)	-1.85 ± 0.10	-4.1 ± 0.1	0.022 ± 0.003
3PEG 1.5 mol/kg $LiClO_4$ 20 wt % Al_2O_3 (1)	-1.57 ± 0.10	-4.1 ± 0.1	0.021 ± 0.003

[a] Also shown are values of the crossover scattering vector Q^*. Numbers in parentheses refer to the numbering of the curves in Figure 3.

silica-filled polymers[20] and in silica aggregates in NaCl solutions.[18,37] The crossover scattering vector Q^* can be interpreted as the inverse of the length scale of the particles forming larger aggregates.[18,20] Here, typically $Q^* = 0.015$ Å^{-1} for the TiO_2-filled samples, which corresponds to a length scale of $2\pi/0.015$ Å $= 40$ nm. This length scale is of the same order of magnitude as the particle diameter (21 nm). For Al_2O_3-filled samples $Q^* = 0.022$ Å^{-1}, which gives a length scale of 30 nm. This smaller length scale is consistent with the smaller size of the Al_2O_3 particles (as compared to TiO_2). The intensity slope of -4 observed at high Q values ($Q > Q^*$) in all samples indicates that the primary particles are uniformly dense with smooth and sharp surfaces.[18] The increasing intensity below Q^* indicates that these primary particles aggregate to larger structures. The power-law behavior with a slope of around -2 in this low-Q region indicates that the aggregates are polymer-like and branched fractal structures. Since no flat plateau is observed in the low-Q limit, a minimum upper length scale of these aggregates can be estimated as $2\pi/0.0015$ Å $= 400$ nm, although it is likely that the aggregates are even larger. If it is assumed that the scattering at large values of Q follows a Porod behavior, then the parameter C of eq 6 can be written as $C = 2\pi(\Delta\rho)^2 S/V$, where S is the total surface area of the particles in the sample volume V. Since the values of C, $\Delta\rho$, and V are known, the surface area S can be calculated and turns out to be 4.4×10^3 cm^2 in the case of 3PEG 10 wt % TiO_2. If it is assumed that the filler material consists of spheres of diameters of ~20 nm, the surface area should be 8.5×10^3 cm^2. The fact that the experimentally observed value of S is only 2 times smaller is in line with the idea of a structure where the primary particles retain their shape but form larger structures.

Further support for the presence of fractal structures can be obtained from an alternative analysis of the experimental data. Teixeira has given an analytical expression for the scattering due to spherical primary particles of radius R forming fractal structures.[38] If the primary particles are assumed to have a size distribution described by a distribution function $N(R)$, the following expression can be given for the scattering cross section

$$\left[\frac{d\Sigma}{d\Omega}(Q)\right]_{coh} = \frac{1}{V}\int_0^\infty N(R)\, S(Q)\, P(Q,R)\, dR \qquad (7)$$

Here, $S(Q)$ is Teixeira's function[38] and $P(Q,R) = V_{part}^2(\Delta\rho)^2|F(Q,R)|^2$, where $F(Q,R)$ is the ordinary form factor for spherical particles, that is[38]

$$S(Q)\, P(Q,R) = \left[1 + \frac{D\Gamma(D-1)\sin[(D-1)\arctan(Q\xi)]}{(QR)^D[1+1/(Q^2\xi^2)]^{(D-1)/2}}\right] \left(\frac{4\pi R^3}{3}\right)^2(\Delta\rho)^2\left(\frac{3[\sin(QR) - QR\cos(QR)]}{(QR)^3}\right)^2 \qquad (8)$$

In this expression ξ represents the length scale of the size of the fractal structures. The 3PEG 10 wt % TiO_2 data were fitted to eqs 7 and 8 assuming a log−normal size distribution for the primary particles, that is

$$N(R) = \frac{N}{C_{LN}}\frac{1}{R^{-p}}\exp\left(-\frac{[\log(R/R_0)]^2}{2\sigma^2}\right) \qquad (9)$$

where N is the number of particles, R_0, σ, and p are parameters determining the size distribution, and $C_{LN} = \sqrt{2\pi}\sigma R_0^{1-p}\exp[(1-p)^2(\sigma^2)/2]$ is a normalization constant chosen so that $\int_0^\infty N(R)\, dR = N$. The fitting was done using the sasfit package developed by one of the authors (J.K.). The fitting was first done with ξ, p, and $\Delta\rho$ fixed (to 400 nm, 0 and 1, respectively) and with N, σ, R_0, D, and a background I_{bk} as free parameters. The contrast $\Delta\rho$ could be fixed to 1 by regarding N as a fitting parameter including both the number of particles, contrast, and possibly also other multiplicative factors. The fitting resulted in a peak radius R_0 of ~6 nm and a rather broad size distribution (full width at half-maximum, fwhm, 7 nm) of the individual particles constituting the fractal structures. These values are not really realistic since the average size, or diameter, of the particles has been specified to be 16−20 nm.[28] However, a fit of almost equally good quality could be produced by fixing the peak radius to 9 nm. The fit is shown in Figure 4. The latter fit resulted in $D = 2.16$, that is, a fractal dimension somewhat greater than in the analysis above, and a width of the size distribution (fwhm) of 6 nm ($\sigma = 0.30$). Thus, the size distribution is still rather broad, as can be seen in the inset of Figure 4. When attempts were made to also fix σ (and hence the width of the size distribution) to lower values, the fit rapidly became worse. Thus, it seems that the size distribution of the primary particles is larger than expected.[28] A possible explanation could be that small spherical clusters of primary particles cannot be distinguished from what appears to be primary particles of larger size. Using the fit result for N, eqs 7 and 8, and the fact that $\Delta\rho$ is known, the number density of primary particles, $n_p = N/V$, can be estimated to be 1.5×10^{15} cm^{-3}. The number density can also be estimated directly. Since the volume fraction of the filler in 3PEG 10 wt % TiO_2 is 0.028, the number density turns out to be 6.7×10^{15} cm^{-3} if the particles are assumed to be of

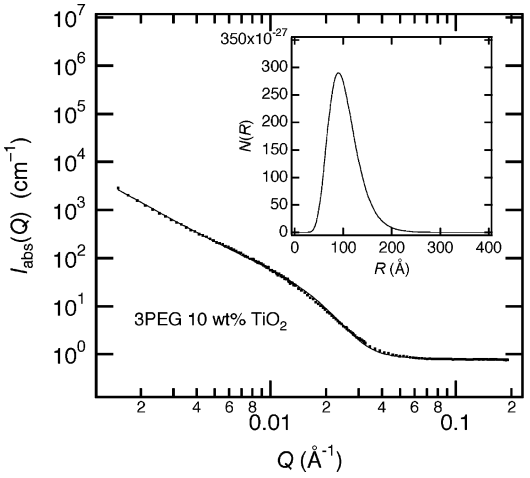

Figure 4. SANS intensity (dots) from 3PEG 10 wt % TiO_2 and curve (solid) fitted to eqs 7−9 with R_0 fixed to 9 nm (ξ fixed to 400 nm, p to 0, $\Delta\rho$ to 1; the fit resulted in $\sigma = 0.30$, $D = 2.16$, and $I_{bk} = 0.79$ cm^{-1}). Some obviously deviating data points were removed prior the curve fitting. The inset shows the resulting size distribution $N(R)$.

equal size with a diameter of ∼20 nm. The fact that the both values of N at least are of the same order of magnitude indicates that the fitting procedure results in physically plausible values of the fit parameters.

To summarize, the two ways of analyzing the data give essentially consistent results, that is, primary particles of a diameter of the order 20 nm that form a branched fractal network with a fractal dimension of around 2.

4. Discussion

From the present SANS measurements it is quite clear that the filler particles aggregate within the base polymer and the polymer electrolyte. The structural picture that emerges can be described as follows: Dense primary particles with smooth and sharp surfaces cluster and aggregate in fractal, polymer-like aggregates. The aggregates consist of branched chains, which are about 40 nm, or 1−2 primary particles, wide in the case of TiO_2 and somewhat narrower in the case of Al_2O_3 filler. The fractal structure extends to length scales of at least 400 nm.

We note that if the intensities from the filled samples (10 wt %) with and without salt in Figure 2a,b are compared, there is no significant difference. This shows that the salt has very little influence on the aggregate structure of the filler. If we compare the low-Q slopes between the 3PEG samples (Table 1), we note that the slope is less steep for samples containing Al_2O_3, indicating that the Al_2O_3 particle aggregates are less branched and more chainlike than the TiO_2 aggregates. Somewhat unexpectedly, the least steep slope ($p = -1.57$) is obtained for the highest Al_2O_3 filler loading. Possibly, this could be related to a higher degree of polydispersity among the entire fractal structures in samples containing Al_2O_3, since it has previously been shown that polydisperse fractal aggregates, with fractal dimension D, may result in slopes less steep than D due to the polydispersity.[38]

The results obtained here, which show that the filler particles aggregate, suggest the formation of percolating networks of filler−particle interface layers. It should be noted that percolation actually may occur already at the seemingly small filler concentrations used in this work (10 wt %, or 3 vol %, TiO_2 or Al_2O_3 filler). For instance, it has been shown that carbon black filled natural rubber becomes conducting at an approximate particle volume fraction of 6%.[23] The insulator−conductor transition in such systems is due to the formation of a percolating, conducting network of carbon black particles.[23] Even smaller percolation thresholds have been observed in composites made of epoxy resin and carbon black (∼4 vol %)[39] and polyurethane or epoxy and graphite (1−2 vol %).[40]

The present structural findings may be of importance for explaining the increased conductivity in nanocomposite polymer electrolytes. One idea that previously has been suggested is that the conductivity enhancement on addition of fillers is due to the formation of percolating interface layers (with higher conductivity) around the filler particles.[15] The interface layer is then thought to be more conducting than the bulk polymer, although the exact mechanism for this remains to be clarified. It is likely to be related to the detailed interactions between cations, filler, and polymer as described by several authors.[7,11−13] The present results provide experimental support for that the particles aggregate in percolating structures. Thus, the structural basis for the conductivity model is supported, although it remains to be proven that the interface layers really have superior conduction properties.

Further indications for the idea that the conductivity increase is due to percolating interface layers comes from earlier quasi-elastic neutron scattering (QENS) results.[41] QENS measurements probe the segmental polymer dynamics that is known to determine the ion conducting properties of ordinary polymer electrolytes without fillers. The faster the dynamics is, the higher is the conductivity. However, it was shown that on addition of filler the polymer dynamics slowed down.[41] Thus, some other mechanism than enhanced polymer dynamics must be the reason for the conductivity increase in nanocomposite polymer electrolytes, such as percolating interface layers.

Similar aggregation or clustering as observed here in polymer nanocomposite electrolytes has been observed in silica-filled polymers.[20] In these kinds of systems, which have been comparatively more thoroughly studied and characterized, it has been found that the morphology often depends crucially on the preparation conditions, for instance pH or surface modification of the filler.[21,24−26] It is likely that the same will apply to nanocomposite polymer electrolytes. The large-scale aggregate structure is probably rather sensitive to different preparation conditions. Details of the different percolating structures may then explain the scatter in conductivity data observed in for instance 3PEG-based composites.[42]

5. Conclusions

The present small-angle neutron scattering studies of TiO_2- or Al_2O_3-filled 3PEG nanocomposite polymer electrolytes show that the filler particles are not well dispersed in the polymer matrix. Instead, the data suggest that the particles aggregate and form fractal, polymer-like structures. The findings provide structural support for the idea that the conductivity enhancement in amorphous nanocomposite polymer electrolytes is due to the formation of lithium conducting pathways in interphase regions forming a percolating network, as suggested in ref 15.

Acknowledgment. This work was performed at the Swiss Spallation Neutron Source, Paul Scherrer Institute, Villigen, Switzerland. Thanks to Degussa for provision of the ceramic powder used in this work. J.S. is Royal Swedish Academy of Science Research Fellow supported by a grant from the Knut and Alice Wallenberg Foundation. A.S.B. thanks the Delft University of Technology for a Senior Post-Doctoral Research Fellowship (2001−2002). This work was financially supported by the Swedish Research Council.

References and Notes

(1) Gray, F. M. *Polymer Electrolytes;* The Royal Society of Chemistry: Cambridge, 1997.
(2) Tarascon, J.-M.; Armand, M. *Nature (London)* **2001**, *414*, 359.
(3) Kumar, B.; Scanlon, L. G. *J. Power Sources* **1994**, *52*, 261.
(4) Quartarone, E.; Mustarelli, P.; Magistris, A. *Solid State Ionics* **1998**, *110*, 1.
(5) Capuano, F.; Croce, F.; Scrosati, B. *J. Electrochem. Soc.* **1991**, *138*, 1918.
(6) Krawiec, W.; Scanlon, Jr., L. G.; Fellner, J. P.; Vaia, R. A.; Vasudevan, S.; Giannelis, E. P. *J. Power Sources* **1995**, *54*, 310.
(7) Croce, F.; Appetecchi, G. B.; Persi, L.; Scrosati, B. *Nature (London)* **1998**, *394*, 456.
(8) Berthier, C.; Gorecki, W.; Minier, M.; Armand, M. B.; Chabagno, J. M.; Rigaud, P. *Solid State Ionics* **1983**, *11*, 91.
(9) Best, A. S.; Ferry, A.; MacFarlane, D. R.; Forsyth, M. *Solid State Ionics* **1999**, *126*, 269.
(10) Wieczorek, W.; Siekierski, M. *J. Appl. Phys.* **1994**, *76*, 2220.
(11) Wieczorek, W.; Florjanczyk, Z.; Stevens, J. R. *Electrochim. Acta* **1995**, *40*, 2251.
(12) Wieczorek, W.; Lipka, P.; Zukowska, G.; Wycislik, H. *J. Phys. Chem. B* **1998**, *102*, 6968.
(13) Croce, F.; Persi, L.; Scrosati, B.; Serraino-Fiory, F.; Plichta, E.; Hendrickson, M. A. *Electrochim. Acta* **2001**, *46*, 2457.
(14) Best, A. S.; Adebahr, J.; Jacobsson, P.; MacFarlane, D. R.; Forsyth, M. *Macromolecules* **2001**, *34*, 4549.
(15) Adebahr, J.; Best, A. S.; Byrne, N.; Jacobsson, P.; MacFarlane, D. R.; Forsyth, M. *Phys. Chem. Chem. Phys.* **2003**, *5*, 720.
(16) Kotlarchyk, M.; Chen, S.-H. *J. Chem. Phys.* **1983**, *79*, 2461.
(17) King, S. M. In *Modern Techniques for Polymer Characterization*; Pethrick, R. A., Dawkins, J. V., Eds.; Wiley: Chichester, 1999; Chapter 7.
(18) McCarthy, D. W.; Mark, J. E.; Schaefer, D. W. *J. Polym. Sci., Part B* **1998**, *36*, 1167.
(19) Beaucage, G.; Rane, S.; Schaefer, D. W.; Long, G.; Fisher, D. *J. Polym. Sci., Part B* **1999**, *37*, 1105.
(20) Zhang, Y.; Ge, S.; Tang, B.; Koga, T.; Rafailovich, M. H.; Sokolov, J. C.; Peiffer, D. G.; Li, Z.; Dias, A. J.; McElrath, K. O.; Lin, M. Y.; Satija, S. K.; Urquhart, S. G.; Ade, H.; Nguyen, D. *Macromolecules* **2001**, *34*, 7056.
(21) Oberdisse, J.; Demé, B. *Macromolecules* **2002**, *35*, 4397.
(22) Wypych, G., Ed. *Handbook of Fillers*, 2nd ed.; ChemTec Publishing: Toronto, 1999.
(23) Karasek, L.; Sumita, M. *J. Mater. Sci.* **1996**, *31*, 281.
(24) Espiard, P.; Guyot, A.; Perez, J.; Vigier, G.; David, L. *Polymer* **1995**, *36*, 4397.
(25) Becker, C.; Kutsch, B.; Krug, H.; Kaddami, H. *J. Sol.-Gel Sci. Technol.* **1998**, *13*, 499.
(26) Rharbi, Y.; Cabane, B.; Vacher, A.; Joanicot, M.; Boué, F. *Europhys. Lett.* **1999**, *46*, 472.
(27) Leezenberg, P. B.; Frank, C. W. *Europhys. Lett.* **1995**, *7*, 1784.
(28) Degussa states that the actual particle size is 16−20 nm. This is based on electron microscopy of 50 000 particles (Degussa, private communication).
(29) Kohlbrecher, J.; Wagner, W. *J. Appl. Crystallogr.* **2000**, *33*, 804.
(30) BerSANS data reduction manual. Keiderling, U.; HMI Berlin.
(31) Strunz, P.; Saroun, J.; Keiderling, U.; Wiedenmann, A.; Przenioslo, R. *J. Appl. Crystallogr.* **2000**, *33*, 829.
(32) Wignall, G. D.; Bates, F. S. *J. Appl. Crystallogr.* **1987**, *20*, 28.
(33) Vachon, C.; Vasco, M.; Perrier, M.; Prud'homme, J. *Macromolecules* **1993**, *26*, 4023.
(34) Vachon, C.; Labréche, C.; Vallée, A.; Besner, S.; Dumont, M.; Prud'homme, J. *Macromolecules* **1995**, *28*, 5585.
(35) Carlsson, P.; Mattsson, B.; Swenson, J.; Torell, L. M.; Käll, M.; Börjesson, L.; McGreevy, R. L.; Mortensen, K.; Gabrys, B. *Solid State Ionics* **1998**, *113−115*, 139.
(36) Orädd, G.; Furlani, M.; Ferry, A. *Solid State Ionics* **2000**, *136−137*, 457.
(37) Schaefer, D. W.; Martin, J. E.; Wiltzius, P.; Cannell, D. S. *Phys. Rev. Lett.* **1984**, *52*, 2371.
(38) Teixeira, J. *J. Appl. Crystallogr.* **1988**, *21*, 781.
(39) Tchmutin, I. A.; Ponomarenko, A. T.; Shevchenko, V. G.; Ryvkina, N. G.; Klason, C.; McQueen, D. H. *J. Polym. Sci., Part B* **1998**, *36*, 1848.
(40) Celzard, A.; Marêché, J. F. *Physica A* **2003**, *317*, 305.
(41) Karlsson, C.; Best, A. S.; Swenson, J.; Howells, W. S.; Börjesson, L. *J. Chem. Phys.* **2003**, *118*, 4206.
(42) Forsyth, M.; MacFarlane, D. R.; Best, A.; Adebahr, J.; Jacobsson, P.; Hill, A. J. *Solid State Ionics* **2002**, *147*, 203.

MA050417V